

## REVIEW ARTICLE

# Parametric evaluation of ultra-low global warming potential fluids used in the integrated solar driven supercritical CO<sub>2</sub> cycle combined with Organic Rankine cycle

R.S. Mishra, Yunis Khan

Department of Mechanical Engineering, Delhi Technological University, New Delhi, India 110042

### Article Information

Received: 12 June 2021  
Revised: 29 June July 2021  
Accepted: 10 July 2021  
Available online: 12 July 2021

### Keywords:

Performance parameters evaluation;  
Organic Rankine cycle;  
Pre-compression CO<sub>2</sub> cycle;  
Solar power tower;  
Ultra-low GWP fluids

### Abstract

World energy demand is growing on a daily basis due to industrial expansion and living standards of people. As a result the use of fossil fuels is constantly growing which contributes to higher carbon emissions in the atmosphere Also the fossil-fuel stocks are decreasing slowly, which leads to the challenge of seeking new energy options to facilitate renewable energy sources In this paper, Performance parameters of solar driven pre-compression cycle sCO<sub>2</sub> and organic Rankine cycle using ultra low global warming potential HFO (hydro fluoro olefins) fluids have been evaluated and comparison with the R134a fluid has been carried out the numerical computation has been carried out and it was found that the thermodynamic performance of the system is increased with the maximum cycle temperature, solar intensity and pre-compressor inlet pressure. Also found the R1336mzz(Z) gave highest exergy for the combined system by 78.06% with 55.0% thermal efficiency and 298.5kW power output at solar irradiation of 950 W/m<sup>2</sup> respectively. Similarly, highest waste heat recovery ratio was found 0.84 for the R1336mzz(Z) fluid was observed as compared with R134a of 0.099 using 95% of second heat exchanger effectiveness. Therefore, Low GWP HFO fluids performed better than the R134a.

©2021 ijrei.com. All rights reserved

## 1. Introduction

Due to industrial development and quality of life, worldwide energy demand is expanding every day. As a result, the usage of fossil fuels is steadily increasing, resulting in increased carbon emissions [1]. But supplies of fossil fuels are slowly diminishing. This brings with it the problem of looking for renewable and safe energy options [2]. A number of traditional power choices are currently used to generate clean and environmentally-friendly electricity, such as biomass, solar, wind and geothermal. In addition, because of its availability, low cost and noise-free operation solar electricity is more suitable for power generation [3, 36,37]. The Solar Power

Tower (SPT) is the new innovation among the several CSP systems. A series of complicated sub-systems including a receiver, a 75-150 m high tower, a thermal storage system (optional), a 50-150 m<sup>2</sup> heliostat field and an energy generation system per heliostat field is included in the SPT network. Sunlight is based on heliostat field receivers, in which high-temperature heat is generated in elevated electricity production or for industry [4]. Several researches have been carried out on SPT-driven cycles, like the combined trans-critical CO<sub>2</sub> cycle and, sCO<sub>2</sub> Brayton cycle, triple combined cycle, sCO<sub>2</sub> recompression cycle, sCO<sub>2</sub> recompression with and without intercooling main compressor, multi-generation hybrid cycle

Corresponding author: R.S. Mishra

Email Address: [hod.mechanical.rsm@dtu.ac.in](mailto:hod.mechanical.rsm@dtu.ac.in)

<https://doi.org/10.36037/IJREI.2021.5509>

[5-9]. Moreover, the sCO<sub>2</sub> cycle is the cycle by which thermal power, geothermal energy, coal energy and natural gas are used from a variety of heat sources [10]. A few studies based on the use of sCO<sub>2</sub> were reported, including Khan and Mishra, [1] who carried out research on the collector of solar parabolic trough coupled with partial sCO<sub>2</sub> and ORC heating. This results the thermal efficiency improved by 4.47% with the implementation of the ORC to the existing partial heating cycle. Besarati and Goswami perform a comparative investigation of the various configurations of the sCO<sub>2</sub> cycle such as part-cooling, recovery cycle, and simple recovery [11]. First the systems were examined separately, and then ORC was utilized as the low cycle and once again tested. They argued that the combined cycle achieved thermal efficiency of more than 50 percent compared to the other cycle. Kim et al [12] have also conducted 12 various sCO<sub>2</sub> cycle configurations in the comparative analysis. One of the outcomes of their findings was that there was a high thermal adaptive project to other cycles in the pre-compression and recompression cycle. The two cycles for future research were also suggested to be combined. Khan and Mishra [13] performed a thermo-economic analysis of the pre-compression cycle combined with organic Rankine cycle. They used the HFO fluids in ORC system. They found that HFO fluids performed better than the HFC fluid. Also in another study Khan and Mishra [14] performed parametric analysis on the recompression cycle with main compressor intercooling sCO<sub>2</sub> cycle they used parallel double evaporator ORC as waste heat recovery cycle. They found after integration of the ORC performance is improved by 6.67%. Further from previous studies it was also found that the combined cycle performance also depends upon the proper working fluids selection for ORC. In this direction several researchers selected the working fluids for the bottoming cycle such as Khan and Mishra [1] considered the six working fluids such as R1224yd(Z), R1233zd(E), R1234ze(Z), R1234ze(E), R1234yf, R1234ze(E), R1243zf and R1234ze(E) for the bottoming ORC of combined solar integrated partial heating sCO<sub>2</sub> cycle. They found that among the all selected working fluids the R1233zd(E) gave the highest performance. Khan and Mishra [15] also considered the five working fluids (R245fa, R236fa, isobutene, isopentane and R227ea) for the bottoming ORC of the combined solar power tower driven pre-compression sCO<sub>2</sub> and ORC. They found that the R227ea showed better performance than the other considered working fluids. Yu, Feng and Wang [16] considered eight working fluids for various source driven ORC. They concluded that the system's thermal performance extremely depends upon the type of working fluids. They generally selected HFC (hydro fluoro carbon) working fluids such as R227ea, R236fa, R236ea, R245fa, R600, R600a, R601, and R601a. Highest thermal efficiency was obtained by the R601 fluid. From the literature survey, it is observed that performance of the pre-compression sCO<sub>2</sub> cycle combined with ORC can be enhanced further by using HFO low global warming potential (GWP) and zero ozone depletion potential (ODP) working fluids in the bottoming ORC. Therefore, present study deals with thermal analysis of the SPT driven

combined power generation cycle. Exergy, thermal efficiencies, output net power and waste heat recovery ratio were considered as performance parameters of the proposed system. A computer program in EES [38] software was made to simulate the system.

Parametric analysis of the proposed combined system was conducted with various HFO working fluids and also performance was compared with the HFC working fluid (R134a). The effects of the system variable such as solar irradiation, maximum cycle temperature, inlet pressure of main compressor and pre-compressor, effectiveness of LTR and heat exchanger-2 on system performance were investigated.

## 2. Description of proposed model

The existing system of an integrated combined cycle comprises of two thermodynamic cycles. The sCO<sub>2</sub> pre-compression cycle as top cycle and ORC bottom cycle respectively. Fig. 1 shows a new combined system power-driven by the solar e power tower. The heat transfer fluid (HTF) (molten salt) circulates throughout in the SPT field. This HTF delivers heat through the first heat exchanger-1 (HX1) (state a-b) to the topping cycle. The pre-compression cycle, via the heat exchanger (state 9-1), takes heat from the SPT through the main turbine (MT), heated sCO<sub>2</sub> that circulates in the pre-compression cycle has extended to get power output (state 1-2). Expanded sCO<sub>2</sub> has a lot of heat goes to the high temperature recuperator (HTR) where it is recovered to heat the sCO<sub>2</sub> stream coming into the first heat exchanger HX1 (state 2-3). After the temperature of the HTR sCO<sub>2</sub> stream is decreased and the difference in temperature of the HTR streams is reduced. In the pre-compressor (PC), the sCO<sub>2</sub> stream was pre-compressed (state 3-4) to prevent pinch point issues. Then the sCO<sub>2</sub> stream enters in the low temperature recuperator (LTR) after the PC temperature and pressure has risen, where heat is recovered by the low temperature stream moving to HTR (state 4-5). second heat exchanger HX2 (state 5-6) has provided this quantity of heat to the ORC due to the sCO<sub>2</sub> stream has a bunch of heat and it travels to the second heat exchanger(HX2) where. sCO<sub>2</sub> compressed in MC again to acquire MT inlet pressure (state 6-7) after the stream of MC sCO<sub>2</sub> continues to the LTR (state 7-8). After that the sCO<sub>2</sub> stream goes to regenerate the HTR (state 8-9). Eventually, to complete the cycle, the sCO<sub>2</sub> stream again goes to the HX1. Come on over to the ORC now through the waste of the top cycle, ORC working fluids take heat via the HX2 and then expand in the organic turbine (OT) (state 10-11). Then the fluid stream moves to the heat rejecting condenser (state 11-12) through the pump, fluid stream pressure again improved (state 12-13). Eventually, it goes back to the second heat exchanger (HX2) to get the heat and then the cycle is completed. The temperature-entropy (T-s) diagram is shown in fig. 2 according to corresponding states

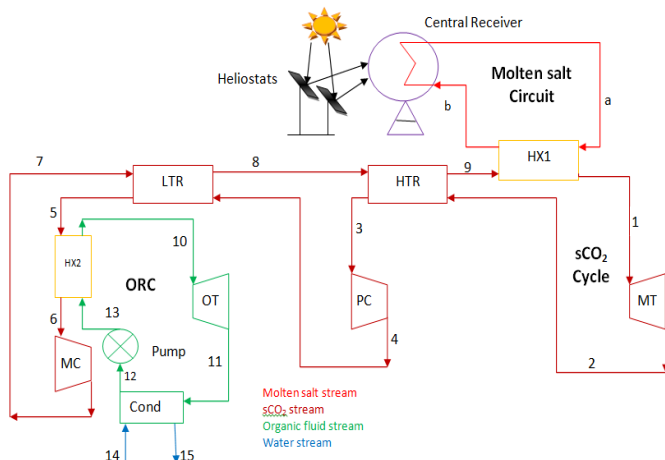


Figure 1: Schematic diagram of solar based combined cycle [13, 22]

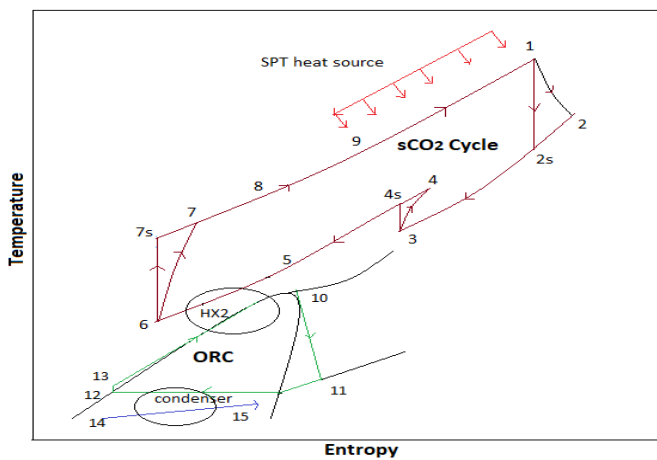


Figure 2: T-s diagram of proposed system [13, 15]

### 3. Thermodynamic analysis

#### 3.1 Assumptions

- To develop thermodynamic model, the following assumptions have been taken.
- All system components are in the thermal equilibrium with the steady state conditions.
- The friction and pressure losses in pipes have been ignored
- Heliostat and receiver parameters have kept constant and assumed input data are displayed in ref. [22].
- Inlet to HX1, temperature of the molten salt has been taken as 700°C [17]
- Due to thermal losses, inlet temperature of MT is 50°C less than temperature of molten salt inlet to the first heat exchanger (HX1).

#### 4. Mathematical modeling

Reference [15] includes a complete mathematical modeling of the existing system; here, only a few helpful equations from

references [5,15] were used for greater understanding. The direct solar heat incidence on a heliostat field [5,15].

$$\dot{Q}_{\text{solar}} = (G_b \cdot A_h \cdot N_h) / 1000 \quad (1)$$

Where  $G_b$  represents solar irradiation ( $W/m^2$ ),  $A_h$  represents single heliostat area ( $m^2$ ), and  $N_h$  represents the number of heliostats. Using first law of thermodynamics, the energy balance equation of the system is as follows:

$$\sum \left(1 - \frac{T_0}{T_Q}\right) \dot{Q}_j - \dot{W}_{c.v} - \sum (\dot{m}_i E_i) - \sum (\dot{m}_e E_e) - \dot{E}D = 0 \quad (2)$$

Where (ED) denotes the rate of exergy degradation and subscript j denotes the thermal characteristic at a specific state. The solar exergy input to the integrated system is calculated as follows [5];

$$\dot{E}_{\text{solar}} = \left(\frac{\dot{Q}_r}{\eta_h \cdot \eta_r}\right) \cdot E_s \quad (3)$$

Where  $E_s$  is the dimensionless maximum usable work, as defined in [5, 15],  $\eta_h$  and  $\eta_r$  are the heliostat and receiver efficiency, respectively.

Using the heat balance equation in the heat exchanger-1; the heat energy collected in the combined cycle from the SPT field is given as follow

$$\dot{Q}_r = \dot{Q}_{\text{HX1}} = \dot{m}_{\text{ms}} \cdot C_{p_{\text{ms}}} \cdot (h_b - h_a) = \dot{m}_{\text{sCO2}} \cdot (h_1 - h_9) \quad (4)$$

In addition, the combined system's exergy assessment should be addressed in this area. After accounting for zero heat losses in each component, an exergy equilibrium Eq. (6) is used to calculate the rate of exergy destruction and exergy for each unit [15]. The rate of total exergy destruction in the combined cycle is computed as;

$$\dot{E}D_{\text{total}} = \dot{E}D_{\text{HX1}} + \dot{E}D_{\text{MT}} + \dot{E}D_{\text{HTR}} + \dot{E}D_{\text{PC}} + \dot{E}D_{\text{LTR}} + \dot{E}D_{\text{HX2}} + \dot{E}D_{\text{MC}} + \dot{E}D_{\text{OT}} + \dot{E}D_{\text{Cond}} + \dot{E}D_{\text{pump}} \quad (5)$$

The net output power Combined cycle is specified as;

$$\dot{W}_{\text{net}} = \dot{W}_{\text{MT}} + \dot{W}_{\text{OT}} - \dot{W}_{\text{PC}} - \dot{W}_{\text{MC}} - \dot{W}_{\text{pump}} \quad (6)$$

The thermal efficiency of Solar powered combined cycle is determined as;

$$\eta_{\text{th}} = \frac{\dot{W}_{\text{net}}}{\dot{Q}_{\text{solar}}} \quad (7)$$

The exergetic efficiency of the combined cycle is computed as [15,19]

$$\eta_{\text{ex}} = 1 - \frac{\dot{E}D_{\text{total}}}{\dot{E}_{\text{solar}}} \quad (8)$$

The thermal efficiency (i.e. first law efficiency) of the

combined cycle is determined as [15];

$$\eta_{th} = \eta_{ex} \cdot \eta_{Carnot} \tag{9}$$

Finally, the waste heat recovery ratio (WHRR) is a measure of how well waste heat can be recovered from a waste heat source. It's calculated as the ratio of a waste heat recovery system's net output power to the maximum amount of waste heat that can be recovered from a waste heat source [20]. It's written like this:

$$WHRR = \frac{W_{net,ORC}}{m_{sCO_2} \cdot (h_5 - h_0)} \tag{10}$$

Where,  $h_0$  is the enthalpy of waste heat available to ORC at environmental temperature

#### 4.1 Working fluids Selection

Working fluids for every system must be deliberately crafted because they have an effect on the environment, financial viability, and long-term viability. In the receiver, molten salt HTF was made up of a mixture of magnesium dichloride (MgCl<sub>2</sub>) and potassium chloride with mass fractions of 32 percent and 68 percent, respectively [5]. This HTF was chosen because, when contrasted to solar salt and liquid sodium (Na), it is the most cost-effective option for the heliostat-driven sCO<sub>2</sub> cycle [25]. Table 2 lists the thermo-physical parameters of molten salt. The choice of working fluid for the ORC is problematic since it loses chemical stability beyond its maximum temperature, yet it achieves optimal thermo-physical qualities at optimum temperatures and pressures [33]. To choose suitable fluids for the study, many factors, such as GWP, thermal stability, and ODP, were investigated. High GWP fluids, such as hydro chlorofluorocarbons (HCFCs), and high ODP fluids, such as chlorofluorocarbons, were excluded from the analysis (CFCs). Regulations such as those of the European Union [27] limited the ODP and GWP to values of less than 1 and 150, respectively.

**Table 1.** Input parameters for simulation of the proposed model [15].

Main turbine inlet pressure	25 MPa [24]
Main turbine inlet temperature	650 °C [5,24]
Inlet pressure of Pre-compressor	5.6–6.8 MPa [17,24]
Main compressor's inlet pressure	7–10.5 MPa [17]
Main compressor's inlet temperature	32–38 °C [17,24]
Main turbine's isentropic efficiency	88% [24]
Main compressor's isentropic efficiency	85% [24]
Isentropic efficiency of Pre-compressor	85% [24]
Effectiveness of heat exchanger	95% [11]
LTR and HTR effectiveness	95% [11]
sCO <sub>2</sub> mass flow rate in topping cycle	1.5 kg/s
Bottoming ORC Mass flow rate	2.5 kg/s
ORC turbine inlet pressure	3 MPa [1,15]
ORC pump's isentropic efficiency	70% [13,14]
ORC turbine's isentropic efficiency	80% [13,14]

Dry and isentropic work is more suited than the other sort of fluid due to high-quality vapour at the expander exit. In the current analysis, the waste heat supply has a low temperature as well. Because of these factors and low temperature applications, ultra-low GWP nine HFO working fluids such as R1234ze(Z), R134a, R1224yd(Z), R1225ye(Z), R1233zd(E), R1234yf, R1243zf, R1234ze(E), and R1336mzz(Z) were selected for the ORC study. The thermal characteristics, protection, and climate conditions of these working fluids are listed in Tables 3(a-c) respectively.

**Table 2:** Heat transfer fluid's thermo-physical properties (MgCl<sub>2</sub>+KCl) [29].

S.No.	Parameters	Values
1	Thermal conductivity	0.39 (W/m-K)
2	Density	1593 (kg/m <sup>3</sup> )
3	Solidification temperature	699 K
4	Specific heat	1.028 (kJ/kg-K)

**Table 3(a):** Thermophysical and environmental properties of working fluids [1,30,35].

Working substance	P <sub>c</sub> (MPa)	T <sub>c</sub> (°C)	T <sub>b</sub> * (°C)
R1234ze(Z)	3.53	150.1	9.8
R134a	4.059	101	-26.1
R1224yd(Z)	3.33	155.5	14
R1225ye(Z)	3.335	106.5	-20
R1233zd(E)	3.57	165.5	18.32
R1234yf	4.597	94.7	-30
R1243zf	3.518	104.44	-25.41
R1234ze(E)	3.64	109.4	-19.0
R1336mzz(Z)	2.903	171.3	33.4

\* T<sub>b</sub> is corresponding to the atmospheric pressure, I: Isentropic, D: dry

**Table 3(b):** Thermophysical and environmental properties of working fluids [1,30,35]

Working substance	Weight (Kg/Kmole)	Type	ODP
R1234ze(Z)	114.04	I	0
R134a	102.03	I	0
R1224yd(Z)	148.5	I	0.00023
R1225ye(Z)	130.5	I	0.00012
R1233zd(E)	130.5	I	0.00024
R1234yf	114.04	I	0
R1243zf	96.05	D	0
R1234ze(E)	114.043	D	0
R1336mzz(Z)	164	D	0

**Table 3(c):** Thermophysical and environmental properties of working fluids [1,30,35].

Working substance	GWP	Lifetime (years)	Security group
R1234ze(Z)	<10	-	-
R134a	1430	14	A1
R1224yd(Z)	0.88	-	A1
R1225ye(Z)	0.87	-	-
R1233zd(E)	1	-	A1
R1234yf	<1	-	A2L
R1243zf	<1	-	A2
R1234ze(E)	6	0.025	A2L
R1336mzz(Z)	8.9	0.0602	A1

4.2 Verification of proposed model

Prior to conducting a thermal analysis of the combined model, it is necessary to check the combined model against past research to confirm that the modeling equations are correctly applied. As a result, the present model was verified using the same input conditions as Khan and Mishra [15] in a prior work, as can be seen in table 4.

Table 4: Validation of combined pre-compression sCO<sub>2</sub> cycle and ORC.

Baseline conditions	Thermal efficiency [15]	Thermal efficiency Current model
P <sub>1</sub> =25MPa, T <sub>1</sub> =650°C, P <sub>6</sub> =6.5 MPa, T <sub>6</sub> = 32°C, P <sub>10</sub> = 3 MPa, η <sub>MC</sub> =0.85,η <sub>MT</sub> =0.88	44.52 %	44.75%

5. Results and discussion

5.1 Performance evaluation with solar heat flux

As the current combined model is powered by a SPT, the effects of solar heat flux on system’s performance must therefore be founded. Using solar heat flux, combined cycle’s exergy efficiency cycle continuously improved. the solar concentrator field efficiently utilizes increased solar heat flux. This contributes to an improvement in the combined cycle’s inlet exergy [1,15]. As solar heat flux increases, the inlet of solar energy to the combined cycle also increases. However, the exergy destruction rate with solar heat flux was not affected. Similarly, the exergy efficiency was increased as shown in Fig. 3. The exergetic efficiency increased from 48.11 to 78.06% using R1336mzz(Z) as working fluid and solar heat flux varied from 400 to 950 W/m<sup>2</sup>. In the other selected working fluids, the R1234ze(Z) produced the lowest exergy efficiency. All HFO working fluids are observed to perform better than the HFC working fluids such as R134a in the present analysis except R1234ze(Z).

Fig. 4 shows the variation of combined cycle’s exergetic efficiency with solar heat flux, the thermal efficiency of the combined cycle has improved. by using R1336mzz(Z) which gives highest thermal efficiency among considered fluids. As solar heat flux increases from 400 to 950 W/m<sup>2</sup>, the highest thermal efficiency was enhanced up to 58.77 per cent because thermal efficiency is directly relating with exergy efficiency, Therefore, as exergy efficiency improved, the thermal efficiency also improved by using solar heat flux

Similarly, the power production of the combine cycle is also increased with solar heat flux as shown in fig. 5. Enhanced solar heat flux increased the enthalpy at the turbine inlet, hence increased work in turbine production increased. the overall output power. At the 950 W/m<sup>2</sup> of solar heat flux with R1336mzz(Z), the highest output power was computed by the developed model at 298.5 kW.

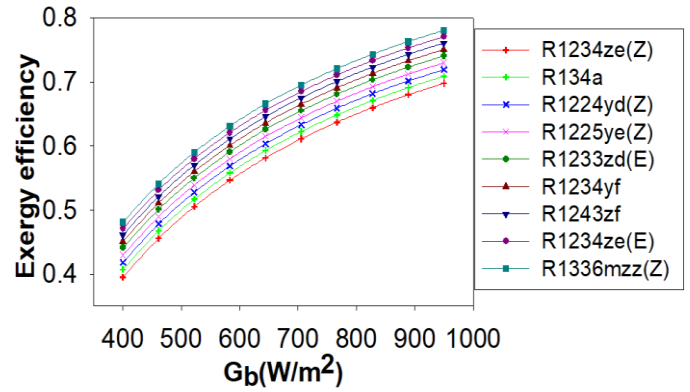


Figure 3: Variation of combined cycle’s exergetic efficiency with solar heat flux

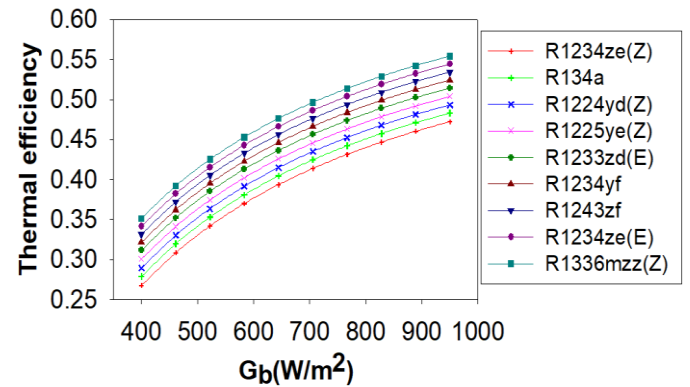


Figure 4: Variation of first law thermal efficiency of combined cycles with solar heat

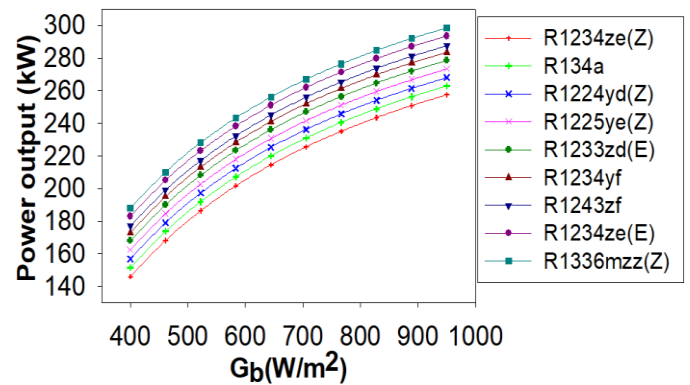


Figure 5: Variation of power output of combined cycles with solar heat flux.

5.2 Performance analysis with maximum cycle temperature

The temperature of the molten salt determines the maximum cycle temperature (MCT) (main turbine inlet temperature). MCT improves as the temperature of molten salt rises. The increasing temperature of both the molten salt will, however, increase heat loss in the solar receiver. Receivers' efficiency suffers as a result [5]. The solar field variables, on the other hand, are held constant in this analysis and are provided in Table 1. As a result, the primary purpose is to examine the cycle's total output. The influence of MCT on system

performance is depicted in fig. 6-8. While evaluating the effects of MCT, the other input data were kept constant, as seen in Table 1. Higher thermal efficiency, however, is not possible due to protection and material limits. Although, under the same solar irradiation, the supercritical carbon dioxide cycle was more efficient at higher input turbine settings than the superheated steam cycle [31].

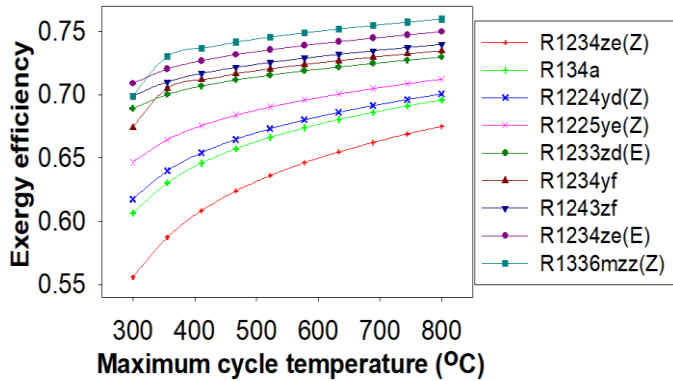


Figure 6: Variation of exergetic efficiency of combined cycle with maximum cycle temperature

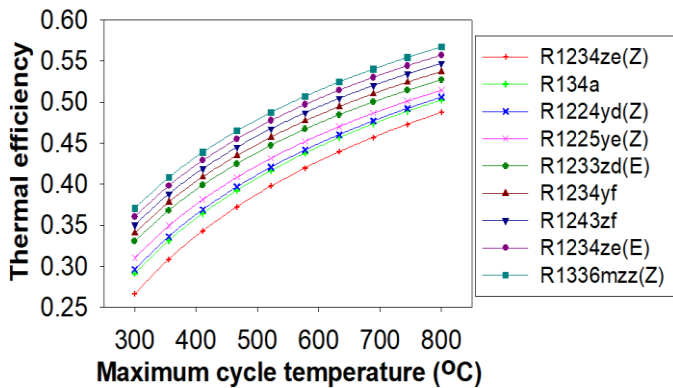


Figure 7: Variation of thermal efficiency of combined cycle with maximum cycle temperature

### 5.3 Performance evaluation inlet pressure of main compressor

In order to test the effect of IPMC, the main compressor's inlet temperature, MT inlet pressure and temperature, and PC inlet pressure were adjusted to 32°C, 25 MPa, 650°C, and 5.6 MPa, respectively. Thermal and exergy efficiency rises with IPMC in the subcritical area, even while pressure is below the critical value of 7.38 MPa, and then declines well beyond critical pressure of CO<sub>2</sub>. This means that there is an ideal pressure when net output power and efficiency has achieved its peak levels. Exergy and thermal efficiencies, as well as net output power, have a bell-shaped curve, as seen in Fig. 9-11. This trend is explained by the fact that higher CO<sub>2</sub> density leads to lower compression power at critical pressure [32]. This correlates to the most net power output and, as a result, the highest thermal and exergy efficiency. At an optimal pressure of 7.81 MPa, R1336mzz obtained the highest thermal and

exergy efficiency and output power of 58.33%, 82.34%, and 287.4 kW, respectively (Z). Fig. 11-13 also illustrate that because the heat available at the combined cycle inlet is constant, efficiency and net power production follow the same pattern.

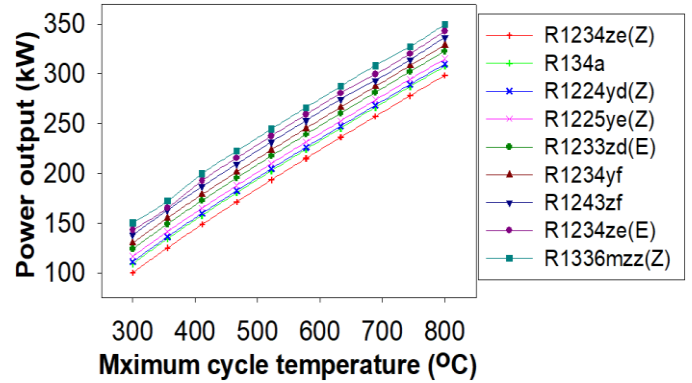


Figure 8: Variation of power output of combined cycle's with maximum cycle temperature.

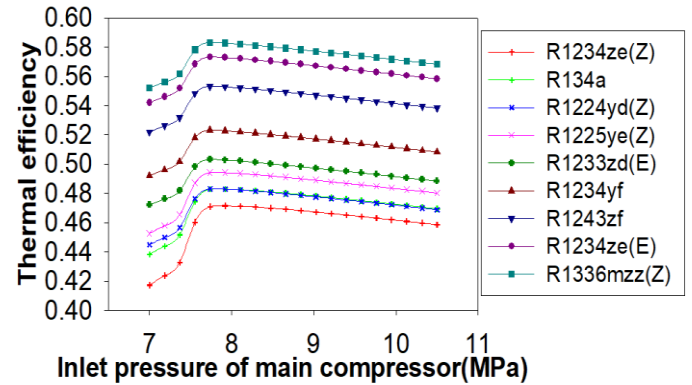


Figure 9: Variation of thermal efficiency of combined cycle with inlet pressure of main compressor

It was also discovered that R1234ze(Z) was evaluated for having the lowest thermal efficiency. The HFO working fluid has also been discovered to perform better than the HFC working fluid

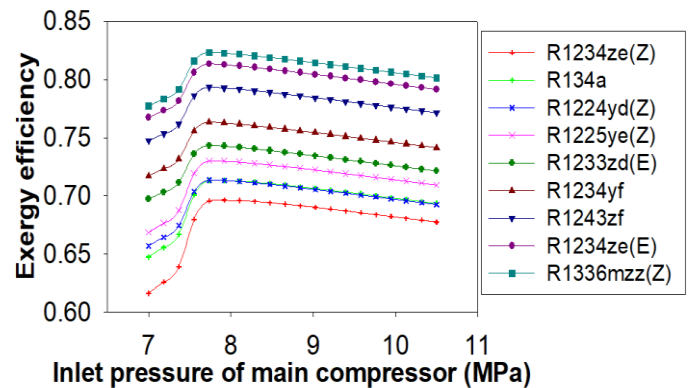


Figure 10: Variation of exergetic efficiency of combined cycle with inlet pressure of main compressor

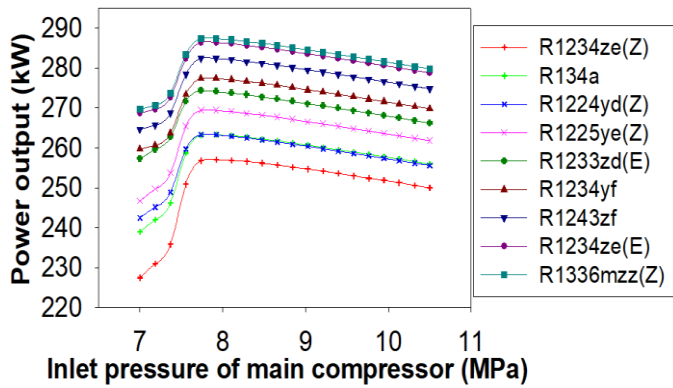


Figure 11: Variation of power output of combined cycle with inlet pressure of main compressor

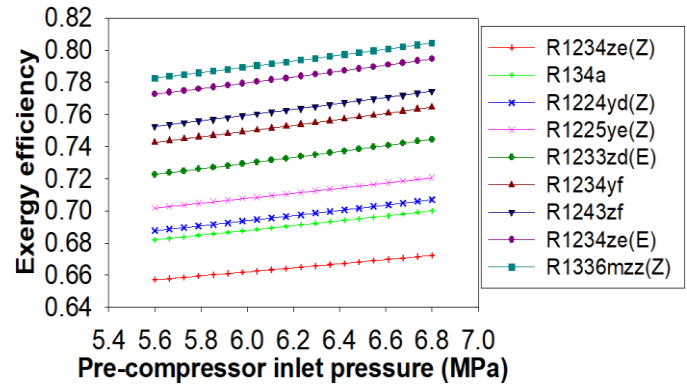


Figure 12: Variation of exergetic efficiency of combined cycle with pre-compressor inlet pressure

#### 5.4 Performance evaluation with pre-compressor inlet pressure

Despite the fact that the focus of this research is on the combined sCO<sub>2</sub> and ORC cycle's functionality. As a result, the effect of the pre-compressor inlet pressure (PCIP) on the system's combined output should be explored. As a result, the impact of PCIP was investigated in order to maintain the stability of other parameters, as shown in Table 1. The system's performance was tested between 5.6 and 6.8 MPa PCIP. Fig. 12-14 show that PCIP enhanced the combined system's thermal, exergy, and net output power efficiencies. Because the density of carbon dioxide increases with pressure at low temperatures. As a result, the PC's input power is reduced. As a result, the combined cycle's net output power is increasing. As a result, the system's thermal and exergy efficiency improves. Fig. 12 shows that the R1336mzz(Z) improved exergy efficiency from 78.26 to 80.45 percent, while PCIP increased from 5.6 to 6.8 MPa. Despite the fact that thermal efficiency and maximum net output power were projected to improve from 54.92 to 56.4 percent and from 291.7 to 294.3kW, PCIP increased from 5.6 to 6.8 MPa with much the same R1336mzz(Z) working fluid, as shown in fig. 13-14. R1336mzz(Z) does have the highest combined cycle efficiency of all the working fluids because of its thermo-physical qualities. As indicated in Table 3, its critical temperatures and pressures are lower than ORC's maximum temperature. R1336mzz(Z) operates in a super-critical environment, according to this. The system delivers the best efficiency when the working fluid is near or above critical condition [33].

#### 5.5 Effects of system variable on waste heat recovery ratio

The goal of this research has been established in this research: to add the bottoming cycle to the fundamental pre-compression cycle. As a result, it's critical to look into a parameter that might be employed in the topping cycle to determine the ORC utility. As a result, fig 15 shows how the efficiency of WHRR with HX2 varies with different working fluids. WHRR has steadily increased as HX2's effectiveness has increased.

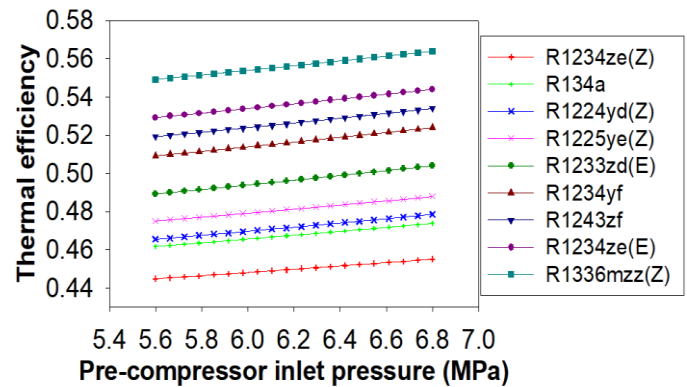


Figure 13: Variation of thermal efficiency of combined cycles with pre-compressor inlet pressure

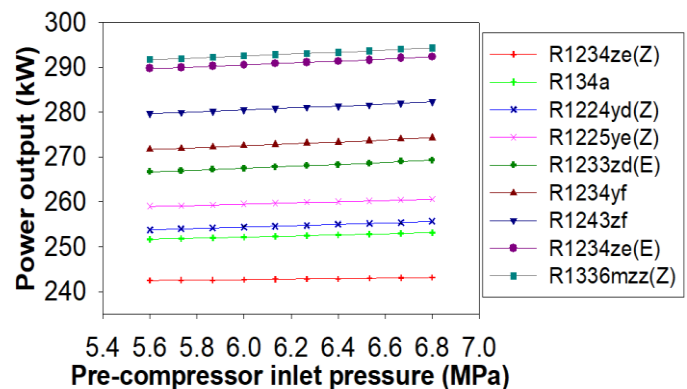


Figure 14: Variation of power output of combined cycle with pre-compressor inlet pressure (PCIP)

The rise in WHRR with HX2 effectiveness can be considered since waste heat recovery in HX2 is boosted with effectiveness, as indicated in the previous section. Maximum WHRR at effectiveness 0.95 was found to be 0.1172, 0.1372, 0.2016, 0.3394, 0.5673, 0.6673, 0.7173, 0.8173, and 0.8673 using R1234ze(Z), R134a, R1224yd(Z), R1225ye(Z), R1234yf, R1234ze(E), R1234yf, R1234ze(E), and R1336mzz(Z). It should also be noted that the WHRR enhancement rates of all working fluids vary. As a result, selecting the proper working fluid for the bottoming ORC is critical for successful waste heat recovery from the topping

cycle. WHRR has grown greatly as a result of the LTR's efficiency, as illustrated in fig 16. When the efficacy of the LTR is improved, more heat is recovered by the sCO<sub>2</sub> cold stream, resulting in a higher WHRR. As a result, the temperature of sCO<sub>2</sub> at the HX2 input drops. In other words, it's reasonable to presume that the low heat is coming from the HX2's input. It lowers the inlet temperature of the ORC turbine. As a result, in the case of organic working fluids, the ORC turbine's output power is increased by the lower inlet temperature [34]. Enthalpy, from the other hand, decreases at state 5 due to lower heat at the HX2 inlet. Using R1234ze(Z), R134a, R1224yd(Z), R1225ye(Z), R1234yf, R1243zf, R1234ze(E), and R1336mzz(Z), the greatest WHRR content was calculated to be 0.0997, 0.1197, 0.1775, 0.3352, 0.56, 0.66, 0.71, 0.8, 0.84 as can be seen in Fig.16.

### 5.6 Effects of system variable on waste heat recovery ratio

The goal of this research has been established in this research: to add the bottoming cycle to the fundamental pre-compression cycle. As a result, it's critical to look into a parameter that might be employed in the topping cycle to determine the ORC utility. As a result, fig. 15 shows how the efficiency of WHRR with HX2 varies with different working fluids. WHRR has steadily increased as HX2's effectiveness has increased. The rise in WHRR with HX2 effectiveness can be considered since waste heat recovery in HX2 is boosted with effectiveness, as indicated in the previous section. Maximum WHRR at effectiveness 0.95 was found to be 0.1172, 0.1372, 0.2016, 0.3394, 0.5673, 0.6673, 0.7173, 0.8173, and 0.8673 using R1234ze(Z), R134a, R1224yd(Z), R1225ye(Z), R1234yf, R1234ze(E), R1234yf, R1234ze(E), and R1336mzz(Z). It should also be noted that the WHRR enhancement rates of all working fluids vary. As a result, selecting the proper working fluid for the bottoming ORC is critical for successful waste heat recovery from the topping cycle.

WHRR has grown greatly as a result of the LTR's efficiency, as illustrated in fig. 16. When the efficacy of the LTR is improved, more heat is recovered by the sCO<sub>2</sub> cold stream, resulting in a higher WHRR. As a result, the temperature of sCO<sub>2</sub> at the HX2 input drops. In other words, it's reasonable to presume that the low heat is coming from the HX2's input. It lowers the inlet temperature of the ORC turbine. As a result, in the case of organic working fluids, the ORC turbine's output power is increased by the lower inlet temperature [34]. Enthalpy, from the other hand, decreases at state 5 due to lower heat at the HX2 inlet. Using R1234ze(Z), R134a, R1224yd(Z), R1225ye(Z), R1234yf, R1243zf, R1234ze(E), and R1336mzz(Z), the greatest WHRR content was calculated to be 0.0997, 0.1197, 0.1775, 0.3352, 0.56, 0.66, 0.71, 0.8, 0.84 as can be seen in fig. 16.

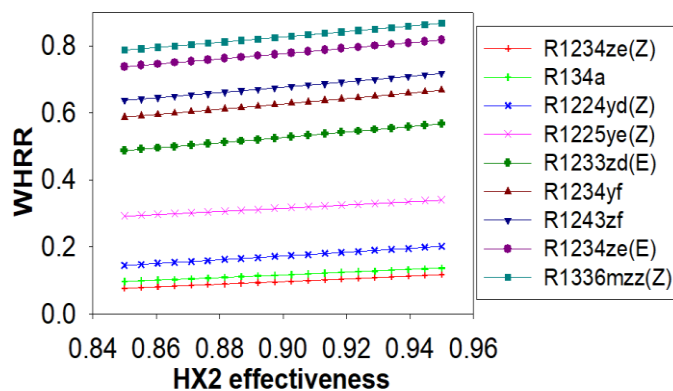


Figure 15: Variation of waste heat recovery rate with HX2 effectiveness

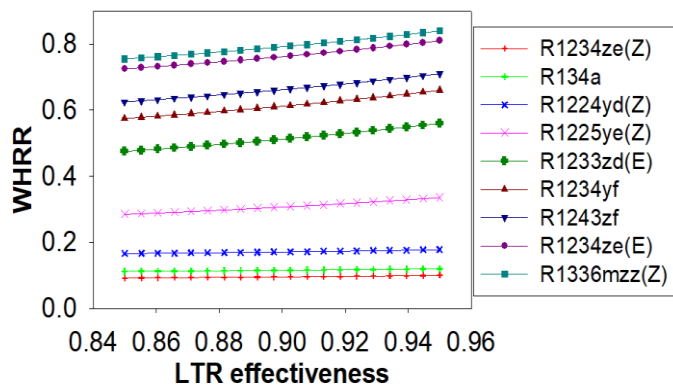


Figure 16: Variation of waste heat recovery rate with LTR effectiveness

## 6. Conclusions

Following conclusions were made from the result discussion;

- Except for R1234ze(Z), which has the lowest performance, all ultra-low GWP HFO working fluids outperform R134. Among all of the working fluids tested, R1336mzz(Z) performed best.
- Using ultra low GWP HFO working fluid R1336mzz(Z), the combined cycle's maximum thermal, exergy, and power production were found to be 55.02 percent, 78.06 percent, and 298.5kW at 950 W/m<sup>2</sup> of solar irradiation, respectively.
- There is a significant difference in WHRR for various working fluids, for example, R1234ze(Z) and R1336mzz(Z) yielded 0.0997 and 0.84 respectively at 0.95 HX2 effectiveness.
  - The HFO working fluid R1336mzz(Z) collected the most waste heat. It was also stated based on the findings that this paradigm is also viable for long-term development.

## References

- [1] Khan Y and Mishra R S. 2020. Parametric (exergy-energy) analysis of parabolic trough solar collector-driven combined partial heating supercritical CO<sub>2</sub> cycle and organic Rankine cycle. Energy sources, part a: recovery, utilization, and environmental effects. doi:10.1080/15567036.2020.1788676.

- [2] Wei L, Zhang Y, Mu Y, Yang X, and Hu X. 2014. Simulation and experimental research of a low-grade energy conversion system using organic Rankine cycles. *Energy Sources, Part A: Recovery, Utilization, and Environmental Effects* **36** (5):537–46.
- [3] Kabira E, Kumar P, Kumar S, Adelodund A A and Kime K. 2018. Solar energy: Potential and future prospects. *Renewable and Sustainable Energy Reviews* **82**: 894-900. doi:10.1016/j.rser.2017.09.094
- [4] Farges O, Béziau J and El-Hafi M 2018. Global optimization of solar power tower systems using a Monte Carlo algorithm: Application to a redesign of the PS10 solar thermal power plant. *Renewable Energy*. **119**:345-353. doi:10.1016/j.renene.2017.12.028.hal-01660563
- [5] Khatoun, S. and Kim M. 2020. Performance analysis of carbon dioxide based combined power cycle for concentrating solar power. *Energy Conversion and Management* **205**: 112416. doi:10.1016/j.enconman.2019.112416.
- [6] Alsagri A S, Chiasson A, Gadalla M. 2018. Viability Assessment of a Concentrated Solar Power Tower with a Supercritical CO<sub>2</sub> Brayton Cycle Power Plant. *Journal of Solar Energy Engineering*. doi:10.1115/1.4043515.
- [7] Maa Y, Morozuyuk T, Liu M, Yan J and J. Liu 2019. Optimal integration of recompression supercritical CO<sub>2</sub> Brayton cycle with main compression intercooling in solar power tower system based on exergo-economic approach. *Applied Energy*. **242**:1134-1154.
- [8] Shukla A K, Sharma A, Sharma M and Nandan G 2018. Thermodynamic investigation of solar energy-based triple combined power cycle. *Energy Sources, Part A: Recovery, Utilization, and Environmental Effects*. doi:10.1080/15567036.2018.1544995.
- [9] Abid M, Adebayo V O and Atikol U. 2019. Energetic and exergetic analysis of a novel multi-generation system using solar power tower. *International journal of exergy*. doi:10.1504/IJEX.2019.100364.
- [10] Ahn Y et al. 2015. Review of supercritical CO<sub>2</sub> power cycle technology and current status of research and development, *Nuclear Engineering Technology* **47**: 647–61.
- [11] Besarati S M, and Goswami D Y. 2014. Analysis of Advanced Supercritical Carbon Dioxide Power Cycles With a Bottoming Cycle for Concentrating Solar Power Applications. *Journal of Solar Energy Engineering* **136**: 010904-1-7. doi: 10.1115/1.4025700
- [12] Kim M.S et al. 2016. Study on the supercritical CO<sub>2</sub> power cycles for landfill gas firing gas turbine bottoming cycle. *Energy* **111**: 893-09.
- [13] Khan Y, Mishra R.S. Thermo-economic analysis of the combined solar based pre-compression supercritical CO<sub>2</sub> cycle and organic Rankine cycle using ultra low GWP fluids. *Thermal Science and Engineering Progress* 2021; 23:100925. doi:10.1016/j.tsep.2021.100925.
- [14] Khan Y, Mishra R.S. Performance analysis of solar driven combined recompression main compressor intercooling supercritical CO<sub>2</sub> cycle and organic Rankine cycle using low GWP fluids. *Energy and Built Environment* 2021. doi:10.1016/j.enbenv.2021.05.004.
- [15] Khan Y and Mishra R S. 2020. Performance evaluation of solar-based combined pre-compression supercritical CO<sub>2</sub> cycle and organic Rankine cycle. *International journal of Green energy*. doi:10.1080/15435075.2020.1847115.
- [16] Yu H, Feng X and Wang Y. 2016. Working Fluid Selection for Organic Rankine Cycle (ORC) Considering the Characteristics of Waste Heat Sources. *Industrial and engineering chemistry research*. doi: 10.1021/acs.iecr.5b02277.
- [17] Reyes-Belmonte M A, Sebastián A, and Romero M. 2016. Optimization of a recompression supercritical carbon dioxide cycle for an innovative central receiver solar power plant. *Energy*. **112** :17–27.
- [18] Cengel Y A and Boles M A. 2004. *Thermodynamics An Engineering Approach* (5th edition), McGraw-Hill publication. New York. USA.
- [19] Parrott J E. 1978. Theoretical upper limit to the conversion efficiency of solar energy. *Solar Energy*. **21**:227–29.
- [20] Kim Y M, Shin D G, Kim C G, and Cho G B. 2016b. Single-loop organic Rankine cycles for engine waste heat recovery using both low- and high-temperature heat sources. *Energy*. **96**:482–94.
- [21] Bejan A, Kearney D W, Kreith F. 1981. Second law analysis and synthesis of solar collector systems. *J. Sol. Energy Eng. Trans. ASME*. **103**:23–28.
- [22] Ho C K. and Iverson B D. 2014. Review of high-temperature central receiver designs for concentrating solar power. *Renewable Sustainable Energy Reviews*. **29**:835–46.
- [23] Wang X et al. 2018. Investigation of thermodynamic performances for two-stage recompression supercritical CO<sub>2</sub> Brayton cycle with high temperature thermal energy storage system. *Energy Conversion Management*. **165**:477–87.
- [24] Neises T and Turchi C 2014. A Comparison of Supercritical Carbon Dioxide Power Cycle Configurations with an Emphasis on CSP Applications. *Energy Procedia*. **49**:1187–96.
- [25] Polimeni S, Binotti M, Moretti L, and Manzolini G. 2018. Comparison of sodium and KCl-MgCl<sub>2</sub> as heat transfer fluids in CSP solar tower with sCO<sub>2</sub> power cycles. *Solar Energy*. **162**:51024.
- [26] Koc, Y., Yaglı H, and Koc A. 2019. Exergy analysis and performance improvement of a subcritical/supercritical Organic Rankine Cycle (ORC) for exhaust gas waste heat recovery in a biogas fuelled Combined Heat and Power (CHP) 520 engine through the use of regeneration. *Energies* **12** (4):575. doi:10.3390/en12040575.
- [27] Moloney F, Almatrafi E and Goswami D Y. 2017. Working fluids parametric analysis for the regenerative supercritical organic Rankine cycle for medium geothermal reservoir temperatures. *Energy Procedia*. **129**:599–606.
- [28] Calm, J.M. 1994. Refrigerant safety. *ASHRAE Journal*. **36**(7):17-26.
- [29] Xu, X et al. 2018. Experimental test of properties of KCl–MgCl<sub>2</sub> eutectic molten salt for heat transfer and thermal storage fluid in concentrated solar power systems. *Journal of Solar Energy Engineering*: **140** (5). 051011.
- [30] Joaquín N. 2017. Experimental study of an Organic Rankine Cycle with HFO-1336mzz-Z as a low global warming potential working fluid for micro-scale low temperature applications. *Energy*. doi: 10.1016/j.energy.2017.05.092.
- [31] Chacartegui R et al. 2011. Alternative cycles based on carbon dioxide for central receiver solar power plants. *Applied Thermal Engineering*. **31**:872–879.
- [32] Blanco M and Santigosa L R. 2017. *Advances in Concentrating Solar Thermal Research and Technology*, Woodhead publishing series in energy (Elsevier). ISBN: 978-0-08-100516-3.
- [33] Kalra C et al. 2012. High-potential power cycles & working fluids for next generation binary supercritical organic Rankine cycle for enhanced geothermal systems. *Proceedings, Thirty-Seventh Workshop on Geothermal Reservoir Engineering*, Stanford University, Stanford, California.
- [34] Dai Y, Wang J and Gao L. 2009. Parametric optimization and comparative study of organic Rankine cycle (ORC) for low grade waste heat recovery. *Energy Conversion and Management* **50**: 576–82.
- [35] Mishra R.S. and Khan Y. 2017. Exergy and energy analysis of modified organic rankine cycle for reduction of global warming and ozone depletion. *International Journal of Research in Engineering and Innovation*. **1**(3), 1-12.
- [36] Mishra R S and Khan Y. 2017. Exergy analysis of orc integrated combined cycle power plant with single pressure heat recovery steam generator. *International Journal of Research in Engineering and Innovation*. **1** (3), 155-162.
- [37] Khan Y and Mishra R S. 2018. Thermodynamic (energy-exergy) analysis of combined cycle power plant for improving thermal energetic and exergetic efficiencies by integration of organic Rankine cycle (ORC). *International Journal of Research in Engineering and Innovation*. **2**(1):86-92.
- [38] Klein S A. 2020. *Engineering Equation Solver (EES)*, Academic Commercial V7.714. F-Chart Software, www.fChart.com.

## Nomenclature

$A_h$	Single heliostat area (m <sup>2</sup> )
$\dot{E}D$	Exergy destruction rate (kW)
$\dot{E}_{solar}$	Solar exergy available combined cycle inlets (kW)
$\dot{E}$	Exergy rate (kW)
$G_b$	Solar irradiation (W/m <sup>2</sup> )
$h$	specific enthalpy (kJ/kg)
$\dot{Q}$	Heat rate in (kW)
sCO <sub>2</sub>	Supercritical carbon dioxide
$\dot{Q}_r$	Heat available at central receiver (kW)

$\dot{Q}_{\text{solar}}$	Sun heat absorbed by heliostat field (kW)	HX2	heat exchanger -2
$s$	specific entropy (kJ/kg-K)	HFC	Hydro fluoro carbon
$\eta_{\text{h}}$	Heliostat efficiency	HFO	Hydro fluoro olefins
$N_{\text{h}}$	Number of heliostat	PCIP	Pre-compressor inlet pressure (MPa)
$\eta_{\text{th}}$	Thermal efficiency	MC	Main compressor
$\dot{m}$	Mass flow rate (kg/s)	CR	concentration ratio
$\eta_{\text{r}}$	Thermal efficiency of receiver	HX1	heat exchanger -1
$\dot{W}$	Power (kW)	IPMC	Inlet pressure of main compressor (MPa)
$\eta_{\text{ex}}$	Exergy efficiency	MCT	Maximum cycle temperature (°C)
$T$	Temperature (K)	HTR	High temperature recuperator
		MT	Main turbine
		LTR	Low temperature recuperator
		SPT	solar power tower
		ORC	Organic Rankine cycle
		WHRR	Waste heat recovery ratio
		OT	ORC turbine

**Abbreviations**

PC	Pre-compressor
Cond	condenser
CFC	chlorofluorocarbon

**Cite this** article as: R.S. Mishra, Yunis Khan, Parametric evaluation of ultra-low global warming potential fluids used in the integrated solar driven supercritical CO<sub>2</sub> cycle combined with Organic Rankine cycle, International journal of research in engineering and innovation (IJREI), vol 5, issue 5 (2021), 275-284. <https://doi.org/10.36037/IJREI.2021.5509>